

# Reversible deactivation of higher-order posterior parietal areas. I. Alterations of receptive field characteristics in early stages of neocortical processing

Dylan F. Cooke, Adam B. Goldring, Mary K. L. Baldwin, Gregg H. Recanzone, Arnold Chen, Tingrui Pan, Scott I. Simon and Leah Krubitzer

*J Neurophysiol* 112:2529-2544, 2014. First published 20 August 2014; doi:10.1152/jn.00140.2014

**You might find this additional info useful...**

---

This article cites 55 articles, 22 of which can be accessed free at:

</content/112/10/2529.full.html#ref-list-1>

Updated information and services including high resolution figures, can be found at:

</content/112/10/2529.full.html>

Additional material and information about *Journal of Neurophysiology* can be found at:

<http://www.the-aps.org/publications/jn>

---

This information is current as of December 5, 2014.

# Reversible deactivation of higher-order posterior parietal areas. I. Alterations of receptive field characteristics in early stages of neocortical processing

Dylan F. Cooke,<sup>1,2\*</sup> Adam B. Goldring,<sup>1,2\*</sup> Mary K. L. Baldwin,<sup>2</sup> Gregg H. Recanzone,<sup>2,3</sup> Arnold Chen,<sup>4</sup> Tingrui Pan,<sup>4</sup> Scott I. Simon,<sup>4</sup> and Leah Krubitzer<sup>1,2</sup>

<sup>1</sup>Center for Neuroscience, University of California, Davis, California; <sup>2</sup>Department of Psychology, University of California, Davis, California; <sup>3</sup>Department of Neurobiology, Physiology, and Behavior, University of California, Davis, California; and <sup>4</sup>Department of Biomedical Engineering, University of California, Davis, California

Submitted 19 February 2014; accepted in final form 14 August 2014

**Cooke DF, Goldring AB, Baldwin MK, Recanzone GH, Chen A, Pan T, Simon SI, Krubitzer L.** Reversible deactivation of higher-order posterior parietal areas. I. Alterations of receptive field characteristics in early stages of neocortical processing. *J Neurophysiol* 112: 2529–2544, 2014. First published August 20, 2014; doi:10.1152/jn.00140.2014.—Somatosensory processing in the anesthetized macaque monkey was examined by reversibly deactivating posterior parietal areas 5L and 7b and motor/premotor cortex (M1/PM) with microfluidic thermal regulators developed by our laboratories. We examined changes in receptive field size and configuration for neurons in areas 1 and 2 that occurred during and after cooling deactivation. Together the deactivated fields and areas 1 and 2 form part of a network for reaching and grasping in human and nonhuman primates. Cooling area 7b had a dramatic effect on receptive field size for neurons in areas 1 and 2, while cooling area 5 had moderate effects and cooling M1/PM had little effect. Specifically, cooling discrete locations in 7b resulted in expansions of the receptive fields for neurons in areas 1 and 2 that were greater in magnitude and occurred in a higher proportion of sites than similar changes evoked by cooling the other fields. At some sites, the neural receptive field returned to the precooling configuration within 5–22 min of rewarming, but at other sites changes in receptive fields persisted. These results indicate that there are profound top-down influences on sensory processing of early cortical areas in the somatosensory cortex.

area 7b; area 5; motor cortex; premotor cortex; cortical deactivation

SENSORY PROCESSING in the mammalian neocortex is traditionally viewed as hierarchical, with “lower-order” cortical fields (or thalamic nuclei) feeding information forward to “higher-order” areas (e.g., Iwamura 1998). Inherent in this theoretical framework is the idea that simple sensory information coded in primary visual cortex (e.g., stimulus orientation) is assembled into complex percepts (e.g., faces) as it passes to higher-order areas (e.g., Orban 2008). Two lines of evidence indicate that this is an oversimplification of a more complex computational network. The first is the presence of feedback connections to earlier processing stages from areas that are considered to be later stages of processing; the second is the effect on neural response properties of these early cortical areas and thalamic nuclei when higher-order fields are lesioned or deactivated.

A network of connections between the somatosensory thalamus, anterior parietal cortex, posterior parietal cortex (PPC),

and other fields includes a diversity of pathways connecting posterior parietal areas 5L and 7b to earlier levels of processing (Fig. 1). This provides a number of alternate routes for information flow, including feedback projections from PPC that could shape or gate neural characteristics of cortical areas providing PPC input.

Little is known about the functional role of feedback from higher-order somatosensory fields or motor cortex on early cortical processing, but feedback does appear to play a significant role at the subcortical level. For example, suppression of neural activity in macaque area 3b (S1) causes substantial enlargement of receptive fields in the ventroposterior nucleus of the thalamus (Ergenzinger et al. 1998). Likewise, deactivation of cat S1 or S2 and rat S1 also changes the response strength and/or the spatiotemporal structure of receptive fields in the somatosensory thalamus (Ghazanfar et al. 2001; Ghosh et al. 1994). The only studies at the cortico-cortical level are those concerning early stages of cortical processing. For example, deactivation of area 3b or 1 (1/2) in macaques and flying foxes results in larger receptive fields in homotopic locations in the contralateral 3b (Clarey et al. 1996). Taken together, studies of the somatosensory system indicate that feedback plays a clear role in shaping the properties of neurons at early stages of processing, which in turn shape feedforward inputs to the very fields providing feedback.

A related finding from our laboratory was the impetus for the present study and a related study described in a companion paper (Goldring et al. 2014). We observed alterations in receptive field size and configuration of neurons in somatosensory area 1/2 of cortex within 60 min of lesioning area 5L (Padberg et al. 2010). This suggested that connections from PPC modulate responses in area 1/2. These changes occurred on a very short timescale, motivating us to study the dynamics of many individual sites' receptive fields during a series of multiple “reversible lesions.” Here we describe the effect of rapid and reversible thermal deactivation of areas 5L and 7b and motor/premotor cortex (M1/PM) on the receptive fields of neurons in area 1/2. In a companion study (Goldring et al. 2014), we describe changes in response properties of area 1/2 neurons during a reversible deactivation of the same parietal and motor fields. These two studies use distinct stimuli to probe distinct aspects of functional organization and neural responses and are the first to probe the dynamics of PPC feedback on the somatosensory network.

\* D. F. Cooke and A. B. Goldring contributed equally to this work.

Address for reprint requests and other correspondence: L. Krubitzer, Center for Neuroscience, 1544 Newton Ct., Davis, CA, 95618 (e-mail: lakrubitzer@ucdavis.edu).

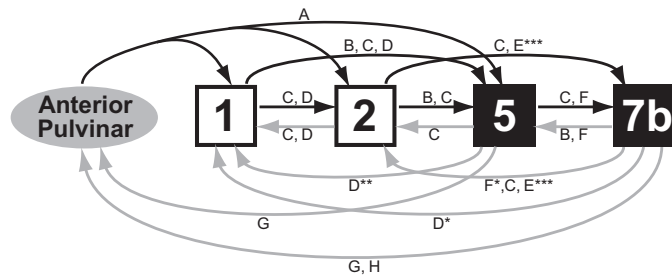


Fig. 1. Selected connections of areas 1, 2, 5, and 7b. Black arrows at *top* are feedforward connections; gray arrows at *bottom* are feedback connections. Gray oval, thalamic nucleus; white squares, anterior parietal fields; black squares, posterior parietal fields. Selected citations for each pathway or group of pathways are provided: A, Padberg et al. 2009; B, Cooke et al. 2013; C, Pons and Kaas 1986; D, Burton and Fabri 1995; E, Rozzi et al. 2006; F, Cavada and Goldman-Rakic 1989; G, Yeterian and Pandya 1985; H, Weber and Yin 1984. \*Face representation only; \*\*retrograde tracer injection in border of areas 1 and 3b; \*\*\*connections to and from area PF, which overlaps 7b. See Table 3 for abbreviations.

## MATERIALS AND METHODS

Six macaque monkeys (*Macaca mulatta*; 2 females, 4 males) weighing between 6.8 and 15.2 kg were used to study the effects of reversible deactivation of posterior parietal areas and/or motor cortex on the receptive field characteristics of neurons within anterior parietal area 1/2. In each anesthetized animal, one to three microfluidic thermal regulators (“cooling chips”; Fig. 2; Cooke et al. 2012) were surgically implanted on the pial surface of areas 7b and 5L and/or on motor cortex. With electrophysiological recording techniques, neural activity was studied in cortical area 1/2 before, during, and after cooling of each region of interest. For multiple sites within each animal (see Tables 1 and 2), receptive field locations and response properties were determined with von Frey hairs as stimuli. Neural responses were also studied quantitatively with computer-controlled stimuli, which is the topic of the companion report. All surgical and experimental procedures were approved by the University of California, Davis Institutional Animal Care and Use Committee and followed guidelines published by the National Institutes of Health.

### Anesthetics and Surgical Procedures

Dexamethasone (0.4–2.0 mg/kg im) was administered preoperatively. Animals were initially anesthetized with ketamine hydrochloride (10 mg/kg im) and intubated, and the saphenous vein was cannulated. Anesthesia was maintained at a surgical level with the inhalant anesthetic isoflurane (0.5–3.0% in 2.0 l/min of O<sub>2</sub>) and supplemental doses of ketamine hydrochloride. In three animals (cases 12-100, 12-149, 12-150), ketamine hydrochloride (2.2–3.6 mg·kg<sup>-1</sup>·h<sup>-1</sup>) was infused intravenously with a syringe pump in order to maintain a constant rate of anesthesia. In the other three animals, a bolus of ketamine (1.1–5.9 mg/kg iv) was given at the beginning of a cooling session to maintain a consistent level of anesthesia within that recording site (see *Recording Epochs* below). In all animals, respiration rate, heart rate, blood oxygenation levels, and temperature were monitored and a continuous drip of 2.5% dextrose in lactated Ringer solution was given at a rate of 6–10 ml·kg<sup>-1</sup>·h<sup>-1</sup> throughout the experiment. Atropine (0.4 mg/kg im) was administered as needed to reduce bronchial secretions and maintain a steady physiological state.

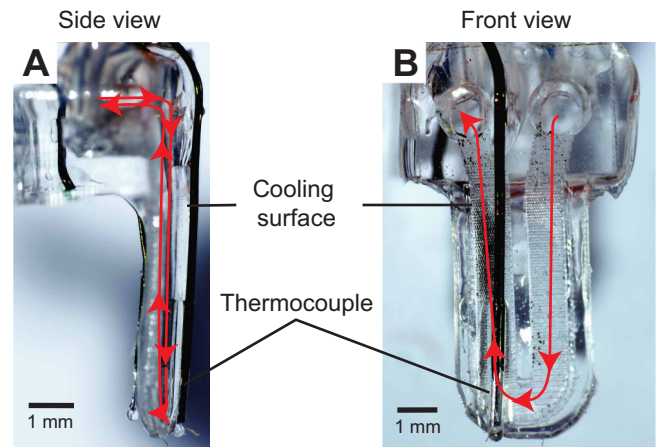
After the animal reached a surgical level of anesthesia, 5% topical lidocaine was placed in the ear canals and the animal’s head was placed in a stereotaxic frame. The skin was cut, and the temporal muscle was retracted to expose the skull. A large craniotomy was made, and the dura was retracted to expose the central and intraparietal (IPS) sulci. The cortex was continuously bathed in sterile saline. The cortical surface was imaged (Nikon D5100 camera with 55-

200-mm Nikon lens and Raynox DCR-250 macro conversion lens) so that the placement of cooling chips and electrode penetrations could be marked relative to vascular patterns and sulci.

Gyral cooling chips (used on area 7b and motor cortex) were gently laid over the area of interest and held in place with tissue adhesive (GLUture) at the adjacent edge of the craniotomy. Once the chips were stabilized, microthermocouples (constructed of 38- to 44-gauge wire, RTD Company) were inserted to an approximate depth of 1,000–1,500 μm into the neocortex directly below the chip through a premade hole in its center (Fig. 2). In some cases microthermocouples were also placed in areas immediately adjacent to the cooling chip or at the chip-cortex interface. This cooling ensemble was then stabilized with a thin coating of dental acrylic (Crosslinked Flash Acrylic, Yates & Bird) that covered a portion of the chip, bone, and microthermocouples.

For cooling chips placed on area 5L in the IPS, Vannas scissors were used to cut the pia mater between the banks of the sulcus. This small opening was gently pried apart with ophthalmic spears, cotton swabs, and blunt forceps until the opening was wide enough to accommodate a cooling chip (Fig. 3C). Placement of sulcal cooling

### Sulcal Cooling Chip



### Gyral Cooling Chip

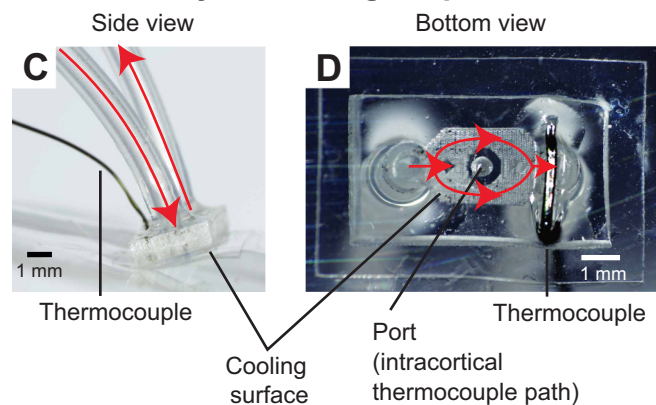


Fig. 2. Selected views of sulcal and gyral cooling chips. Chilled ethanol is passed through silicone tubing and fed into a microchannel just below the cooling surface opposed to the cortex. Red arrows denote coolant flow. A and B: side view (A) and front view (B) of a cooling chip that can be inserted into a sulcus to cool regions such as area 5L. C and D: side view (C) and bottom view (D) of a cooling chip that can be placed on a gyrus to cool regions such as area 7b and M1/PM. A port in the center of the gyral cooling chip allows intracortical temperature to be read via a microthermocouple inserted through the port to a given cortical depth. Indwelling microthermocouples in both types of cooling chip measure the temperature at the interface between cortex and the cooling surface.

**Table 1.** Cases: deactivation tests by region cooled and effect of cooling

Case	Area Cooled (mm <sup>2</sup> )	Deactivation Tests	
		Response change/total	% Changed
11-186	5L (21.0)	2/9	22.2
12-12	5L (6.7)	2/2	100.0
	7b (39.3)	2/3	66.7
	M1 (22.2)	1/2	50.0
	Total	5/7	71.4
12-59	7b (12.1)	8/20	40.0
	M1 (19.0)	0/3	0.0
	Total	8/23	34.8
12-100	7b (6.8)	0/1	0.0
	M1 (4.6)	0/2	0.0
	Total	0/3	0.0
12-149	5L (13.7)	4/9	44.4
	7b (6.8)	3/7	42.9
	M1 (6.8)	1/5	20.0
	Total	8/21	38.1
12-150	7b (6.8)	8/9	88.9
Total across 6 cases			
	5L	8/20	40
	7b	21/40	52.5
	M1	2/12	16.7
Total for all cases, all cooling locations		31/72	43.1

Area cooled is surface area of cooling footprint on cortex. Sites with “changed” response are defined as those with any alteration in the borders of the receptive field on the hand when comparing the receptive field during baseline epoch with that observed during any of the following epochs (cool, rewarm 1, rewarm 2). Up to 3 deactivation tests (cooling of areas 5L and 7b and M1) could be conducted at a single recording site; therefore the deactivation test totals here are often greater than the totals for recording sites examined with cooling in Table 2 (e.g., grand totals of 72 and 55, respectively).

devices was only possible in three animals where the vascular pattern was optimal for this procedure. Cooling chips were placed with the cooling surface facing area 5L and an insulated surface facing the adjacent posterior wall of the IPS. The chip was temporarily stabilized against and glued to a piece of polydimethylsiloxane (PDMS) on the gyral surface. When possible, microthermocouples were placed in the anterior and/or posterior bank of the sulcus immediately adjacent to the cooling device and the entire ensemble was held in place with acrylic. The location and size of gyral and sulcal cooling chips are shown in Fig. 3C, Fig. 4B, and Fig. 5 for different monkeys; Fig. 3 also shows the estimated extent of the inactivated tissue as determined from thermal maps in previous studies (Cooke et al. 2012).

**Cooling Chips**

The design, fabrication, and functional properties of these devices have been described recently by our laboratory (Cooke et al. 2012). Briefly, cooling chips are fabricated from PDMS and silicone tubing and are operated by pumping chilled ethanol through the tubing. Since this initial publication, a new, more compact design, fabricated with laser cutting, has been developed. Most notably, newer chips have smaller cooling footprints than older chips. During pilot testing and in this experiment, this new design functioned similarly to the original, albeit more efficiently, requiring lower coolant flow rates to achieve the same cortical temperature. As both devices were controlled via thermal feedback (see below), there was no practical difference in operation, although the smaller dimensions of the new design made surgical placement easier. This device has an integrated microthermocouple that measures temperature at the interface between chip and cortex. For all cooling chips, temperature was measured at one to three locations around the cooling device. As described previously,

cortical temperature was controlled by varying the coolant flow rate with a computer interfaced with the microthermocouple. Steady-state temperature could be maintained within ±0.3°C for over an hour, although the cooling sessions described here were much shorter. Table 1 lists the cooling footprint for each cooling device used. The area of the cooling footprint of our gyral devices ranged from 4.6 to 39.3 mm<sup>2</sup>. Sulcal device cooling footprints ranged from 5.7 to 21.0 mm<sup>2</sup>. The extent of the effective cooling region or deactivation is limited to the cortex directly adjacent to/below the cooling footprint (Cooke et al. 2012).

**Cortical Areas Cooled**

The placement of our cooling chips was based on sulcal landmarks that have been well established for demarking cortical regions of interest. Area 5L was recently mapped in our laboratory with multiunit electrophysiological recording techniques (Seelke et al. 2012). Although the internal topographic organization was demonstrated to be highly variable, the location of area 5L, on the rostral bank of the IPS extending 1.5 cm from the lateral tip of the sulcus, was stable across animals (Figs. 3 and 4). The hand/forelimb representation in the primary motor/premotor area (M1/PM) occupies a large amount of cortex and can be reliably estimated using several landmarks (Kambi et al. 2011) including the central sulcus, the precentral dimple, the IPS, and the electrophysiologically defined hand representations in anterior parietal somatosensory cortex. M1 is located within the rostral bank of the central sulcus (near the dorsal lip) and wraps onto the precentral gyrus; PM is immediately rostral to M1 on the precentral gyrus. The hand/forelimb representation in both of these fields is just below the superior precentral dimple. Although the map of body movements within M1 is fractured in mammals including macaque monkeys, the hand/forelimb motor maps are at the same mediolateral level as the hand representations in areas 3a, 3b, 1, and 2, which are accurately estimated using the tip of the IPS and postcentral dimple and were confirmed by our recordings within area 1/2. Finally, area 7b, located on the inferior parietal lobule caudolateral to the tip of the IPS, has been described in a number of electrophysiological and anatomical studies (Hyvärinen and Poranen 1974; Leinonen et al. 1979; Lewis and Van Essen 2000; Mountcastle et al. 1975; Preuss and Goldman-Rakic 1991). Although this relatively large posterior parietal field has been further subdivided (Gregoriou et al. 2006; Pandya and Seltzer 1982; Rozzi et al. 2006, 2008), we could not determine these subdivisions using sulcal patterns. Figures 3–5 provide examples of chip placement in the three areas cooled. See Table 1 for the number of chips used in each animal, which ranged from one to three; cooling chips were never run simultaneously.

**Recording Epochs**

For the purposes of analyses presented below there were three or four recording epochs for each site tested (Fig. 3B): 1) “baseline” epoch—

**Table 2.** Cases: recording sites by location in area 1 or 2

Case	Recording Sites (sites examined with cooling/total sites)			
	Area 1	1/2 Border	Area 2	Total
11-186	8/33	1/9	0/9	9/51
12-12	3/15	0/6	0/6	3/27
12-59	8/30	8/21	6/40	22/91
12-100	0/0	3/9	0/21	3/30
12-149	5/24	1/13	3/17	9/54
12-150	6/10	3/7	0/0	9/17
Total across 6 cases	30/112	16/65	9/93	55/270

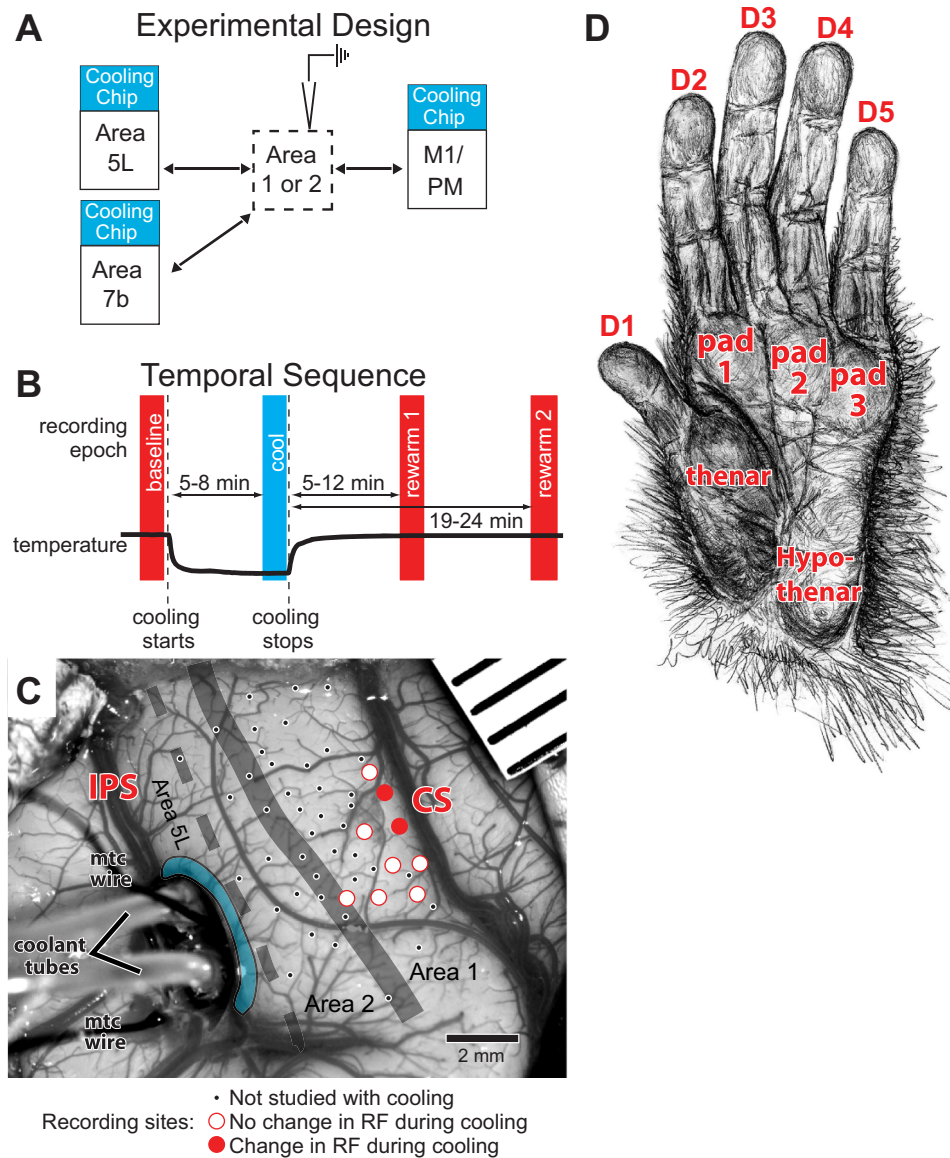
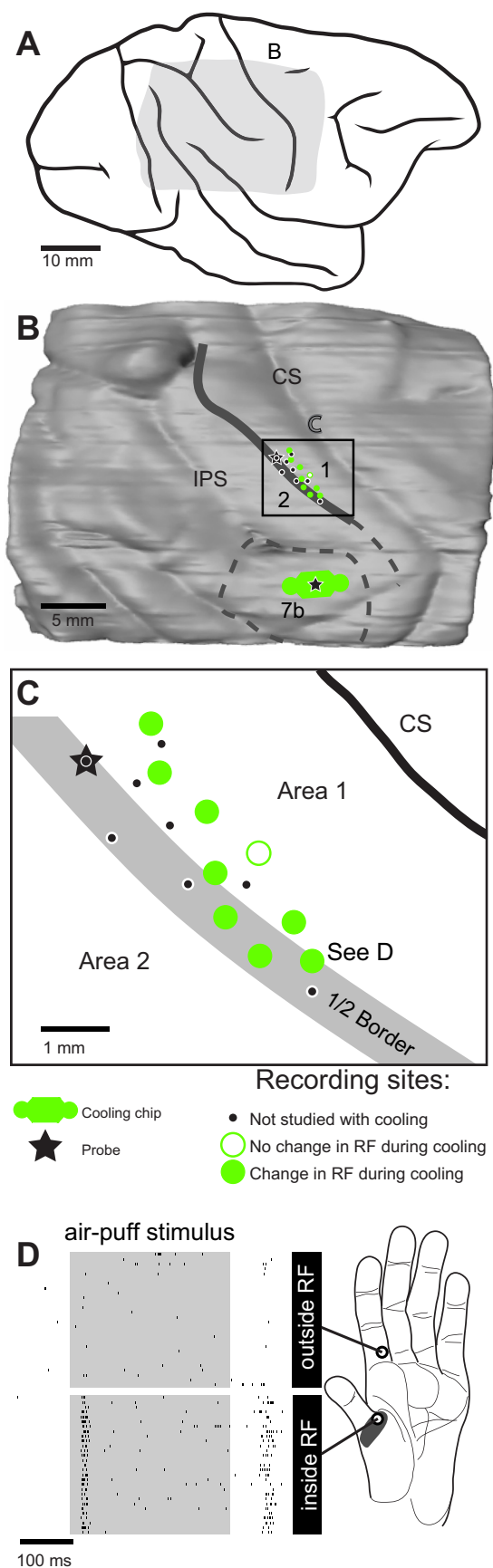


Fig. 3. *A*: schematic of experimental design showing a recording electrode in area 1 or 2 while different fields (5L, 7b, M1/PM) are deactivated one at a time with cooling. Arrows indicate neural connections that may supply feedback directly or, via the thalamus to earlier sensory processing in area 1/2, feedback that is disrupted during cooling. *B*: temporal sequence of the 4 recording epochs (baseline, cool, rewarm 1, rewarm 2) relative to the start and stop of cooling (vertical dashed lines). Thick black trace is a representative plot of cortical temperature. *C*: photograph of a craniotomy with a sulcal cooling chip placed in the intraparietal sulcus (IPS) directly adjacent to a portion of area 5L (to right of the device) in case 11-186. Coolant tubes and microthermocouples (“mtc wire”) extend leftward from the device. Microthermocouples are on the cooling chip itself and in the caudal bank of the IPS. Blue region rostral to the cooling chip is an estimate of the visible cooled area based on previous studies in which the spread of effect was determined (Cooke et al. 2012). Our previous testing indicates that this lateral margin of 0.5–1.0 mm, with effective cooling to the deeper layers of cortex, represents the estimate for both sulcal and gyral cooling devices. Cooled cortex also includes tissue adjacent to the chip on its rostral face extending out of sight ~5.5 mm into the IPS. Recording sites are marked on the cortex: small black dots, sites not studied with cooling; open red circles, no change in receptive field (RF) during or after cooling; solid red circles, change in RF during or after cooling. Mapped region (small dots) extends from the representation of the hand/face border laterally to the forearm medially, with the hand representation in between. All studied sites (large circles) in this case are in area 1 or the area 1/2 border (thick gray line). Dashed line is estimated border between areas 2 and 5L. Red labels are sulci. Rostral is to the right and medial is up. *D*: anatomically correct drawing of the hand with divisions of the palm and digits marked. Drawing by M. K. L. Baldwin. See Table 3 for abbreviations.

immediately before cooling began; 2) “cool” epoch—after the cooled region reached and maintained the target temperature (20–25°C in cortex or 2°C at the chip-cortex interface) for several minutes, usually 5–8 min after cooling was initiated; 3) “rewarm 1” epoch—after the cooled region temperature returned to baseline temperature, usually 5–12 min after cooling ceased; and 4) in 3 animals, “rewarm 2” epoch—a later period, usually 19–24 min after cooling ceased. This final epoch was examined to assess the stability of the receptive field for a period after cortex was rewarmed. Testing during each epoch usually lasted 5–10 min.

#### Electrophysiological Recordings

During each cycle of three or four epochs, electrophysiological recordings were made at a single site in the hand representation of area 1/2 with epoxy-coated tungsten electrodes (0.2–1.1 M $\Omega$ , tip exposures < 30  $\mu$ m; A-M Systems, Sequim, WA). Electrodes were lowered to a depth of 1,000–1,200  $\mu$ m with a micromanipulator (Kopf Instruments, Tujunga, CA), and extracellular activity from neural clusters was amplified and filtered (model 1800 amplifier, A-M



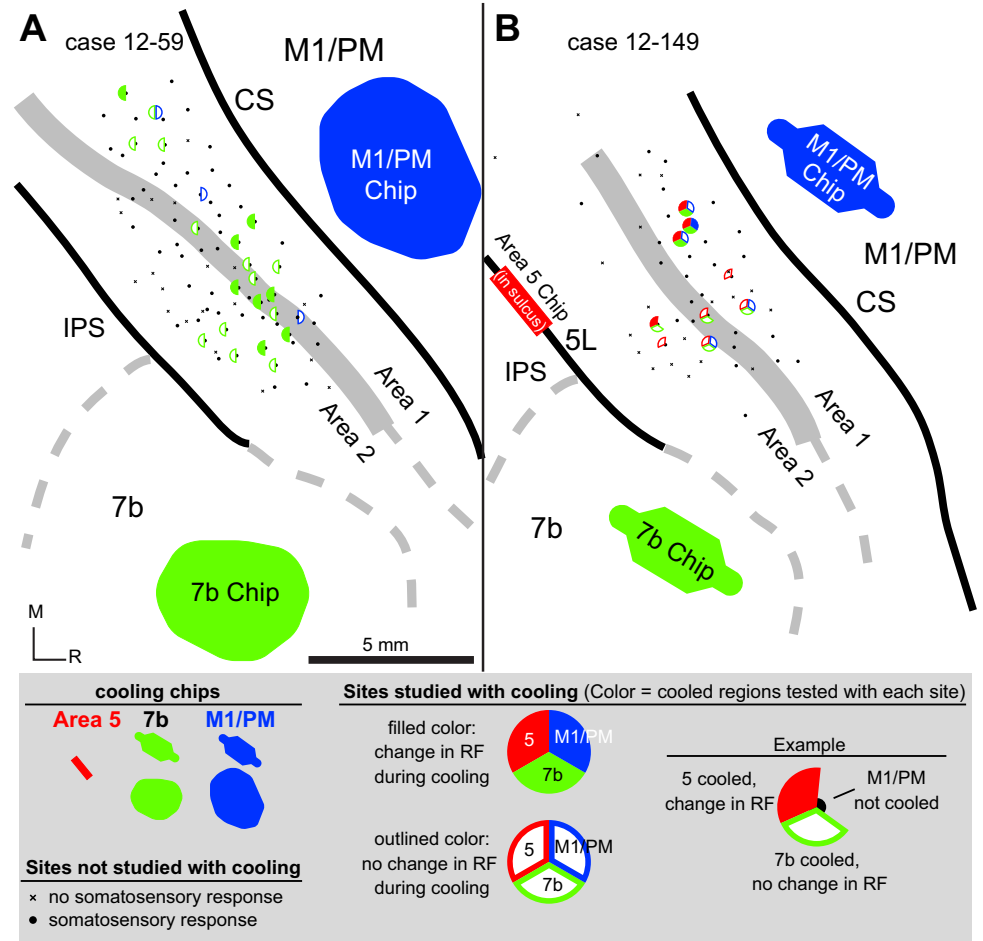
Systems), monitored through a loudspeaker, and visualized on a computer monitor. Each electrode penetration was marked on a digital image of the cortex for later alignment with histologically processed tissue (see below). Once the electrode was lowered to the appropriate depth, we quickly determined the strength of the response by manually stimulating portions of the hand and forelimb. We studied a total of 270 sites across the six animals. Recording sites in which there were strong responses to stimulation of the hand throughout the recording epochs (55 total) were used in our analysis and are reported here. The anatomical locations of each of these 55 sites were reconstructed, and we found that 30 were in area 1, 9 were in area 2, and 16 were located on the border between the two areas and could not reliably be assigned to one or the other (see Table 2).

*Tactile Stimulation and Receptive Field Definition*

Once we identified a site for further exploration, we mapped the cutaneous receptive field, using fine probes, brushes, and von Frey hairs. These methods are similar to those used previously in our own laboratory and those of others (e.g., Padberg et al. 2010; Pons et al. 1985). Deep receptors of the skin and muscle were stimulated by light to hard taps, muscle squeezes, and joint manipulation. Sites in which neurons responded only to deep stimulation of the skin were not studied further. Cutaneous receptive fields for neurons at each site were diagrammed on drawings of the body. Figure 4D shows such an illustration as well as quantitative neural responses to an air-puff stimulus inside and outside the receptive field, a stimulus used in the companion article, where these stimuli are compared (Goldring et al. 2014). Once a receptive field was determined, further stimulation during successive cooling epochs was made with the finest von Frey hair that produced a strong response {probe diameter 0.102–1.143 mm, corresponding to handle labels 2.44–6.65 [ $\text{Log}_{10}(10\text{-mg of force})$ ] or a force of 0.028–447 g}. The same investigator that defined the baseline receptive field also defined all subsequent receptive field boundaries for recordings at that site. Therefore, the individual defining the receptive fields was not “blind” to the experimental condition; blind coding would have required additional catch epochs, adding significantly to the time during which anesthetic plane and neural isolation would have to have been maintained, reducing the number of sites studied. Having a single experimenter defining receptive fields, however, meant that the individual was able to precisely judge

Fig. 4. Reconstruction of recording sites relative to architectonically defined boundaries for case 12-150. *A*: drawing of the dorsolateral aspect of cortex after fixation. Shading indicates region shown in *B*. *B*: 3-dimensional reconstruction showing the region of cooling and mapping in these studies. The reconstruction, generated with Amira software, combines sulci, architectonic boundaries, electrode penetrations, and the location of the cooling chip in area 7b. The cortical surface is derived from outlines of tissue imaged during sectioning. Architectonic boundaries (dark gray line) drawn from Nissl-stained sections were locally aligned to the block-face images to remove distortion. Thickness of the boundary line and the sites within it correspond to the area 1/2 border region used in the analysis (Table 2). Dashed lines depict estimated areal boundaries. Black box indicates region shown in *C*. *C*: recording sites in area 1 and on the border of area 2. Open green circles, no change in RF during or after 7b cooling; filled green circles, change in RF during or after 7b cooling; star, fluorescent fiducial probe for aligning functional data to histologically processed tissue. *D*: comparison of hand-mapped RF (gray shading on hypothenar pad) and multiunit neural response to 300-ms air-puff stimuli used in companion paper (Goldring et al. 2014). Neural responses were recorded from area 1/2 site marked “See D” in *C*. Air puffs were presented alternately at 2 locations on the hand (open circles), one of which was inside the RF. Gray boxes on rasters indicate timing of stimulus. Rasters show robust on and off responses to air-puff stimulation inside the hand-mapped RF on the hypothenar pad (*bottom*), but not to air-puff stimulation on proximal D2, outside of the hand-mapped RF (*top*). Conventions as in Fig. 3.

Fig. 5. Reconstruction of recording sites relative to cooling chip locations, sulci, and architectonically defined area 1/2 boundary for 2 cases (12-59, A; 12-149, B) shown at the same scale. Small black dots, recording sites responsive to somatosensory stimulation but not studied with cooling; ×, unresponsive recording sites not studied with cooling. Cooling chip footprints are color-coded by cortical field (red, area 5; green, area 7b; blue, M1/PM). Sites tested with cooling are marked with colors corresponding to the area(s) cooled: solid color indicates a change in RF as a result of cooling the area of the same color; color outline indicates a site tested with cooling of the corresponding area but no change in RF. Thick gray line is area 1/2 border. Dashed gray lines are estimated areal borders. Medial (M) is up and rostral (R) is to the right.



whether the receptive field boundaries had shifted using the same criteria of stimulation and response strength.

*Histology*

After 1–3 days of electrophysiological mapping experiments, animals were given a lethal dose of pentobarbital sodium (>60 mg/kg iv) and were perfused transcardially with phosphate-buffered saline (PBS) followed by 4% paraformaldehyde in PBS and then with 4% paraformaldehyde with 10% sucrose in PBS. The brains were then removed, and the cortex was separated from the underlying brain structures and the cerebellum. The brain tissue was then placed in a 4% paraformaldehyde-20% sucrose solution for up to 48 h or was placed directly into a 30% sucrose solution in phosphate buffer until the brain sank (48–72 h). The entire hemisphere, or a blocked portion of the brain that included motor, somatosensory, and posterior parietal cortices, was cut on a freezing microtome in the horizontal plane at a thickness of 50 or 60 μm. Block-face images (Nikon D5100) of each section were taken during cutting for use in three-dimensional (3D) reconstruction of the tissue (Fig. 4). Tissue sections were saved in series of three, four, or five, and at least one series was processed for Nissl substance.

*Combining Electrophysiological and Histological Data*

Block-face images of all cortical sections were imported into Amira software (Visualization Sciences Group, Burlington, MA) in order to create a 3D reconstruction of the tissue block (Fig. 4B). The 3D reconstruction was aligned to images of the brain surface taken during the terminal experiment with Adobe Illustrator, which allowed us to confirm electrode and cooling chip sites.

Cortical borders of areas 3b, 1, and 2 were determined with Nissl-stained sections (Fig. 6). These architectonic areas and their relation to electrophysiological recording data have been described in detail in previous studies in macaque monkeys by our own and other laboratories (e.g., Nelson et al. 1980; Padberg et al. 2009, 2010; Pons et al. 1985; Seelke et al. 2012; Sur et al. 1984). Briefly, area 1 contains

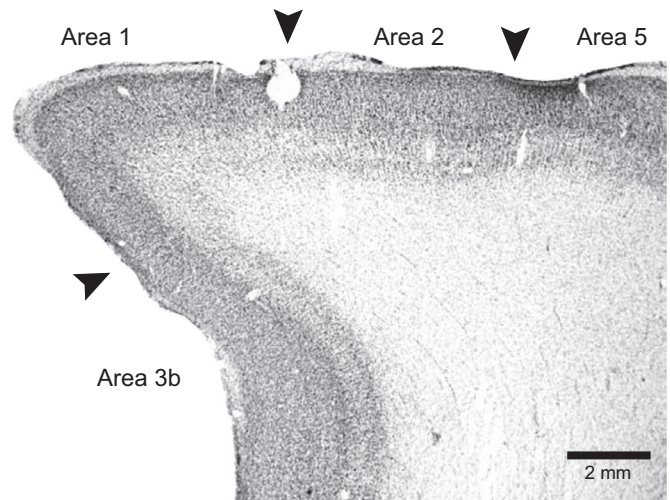


Fig. 6. A horizontal section stained for Nissl from case 12-150. Architectonically defined boundaries (marked by arrowheads) of anterior parietal fields 3b, 1, and 2 are readily defined by their characteristic laminar appearance. All of these cytoarchitectonically defined boundaries have been related to functionally defined cortical areas.

a moderately dense layer 4 and a somewhat lighter-staining layer 6. This is in contrast to area 3b, located rostrally in the caudal bank of the central sulcus, in which both layers 6 and 4 stain darkly and neurons are densely packed. Area 2 abuts the caudal boundary of area 1 and is distinguished by a thickening of layer 4 and increased density in layer 6. Area 5L adjoins the caudolateral boundary of area 2 and is distinguished by thickening of layers 4 and 6 and a reduction in the density of these layers.

Images of Nissl-stained sections were taken with a Microfire camera (Optronics, Goleta, CA) fitted to a Nikon E400 microscope. To facilitate the alignment of Nissl sections with corresponding block-face images, minor distortions introduced to the tissue during histological processing and mounting were corrected by aligning corresponding blood vessels and thus digitally stretching or compressing the features of the intervening tissue with the envelope mesh tool in Adobe Illustrator. These corrected images were imported to the 3D Amira reconstruction in order to project the anatomically determined borders, electrode penetration tracks, and fluorescent fiducial probe locations onto the cortical surface (Fig. 4C). This process was validated by the location of the fiducial probe and observations that electrode track locations in our 3D reconstructions coincided with electrode sites marked on the photograph of the cortical surface taken during experimental procedures *in vivo*. Photographs of tissue sections were adjusted for brightness and contrast with Adobe Photoshop but were otherwise unaltered.

#### *Analysis of Changes in Receptive Fields*

We quantified changes in the extent of the receptive field by dividing the area of the receptive field during later epochs (cool, rewarm 1, rewarm 2) by the area of the receptive field during the baseline epoch. Drawings of receptive field extent on the contralateral hand and arm were digitized, and the area of each receptive field was measured with Adobe Illustrator CS2 (Adobe Systems). We also quantified change in receptive fields between epochs with an “overlap index” (Merzenich et al. 1983; Padberg et al. 2010), which was defined as the area of overlap divided by the area of the geometrical union (merger of the 2 shapes into 1). A receptive field with a change in position but not size would show zero expansion (first metric) but a decreased overlap index. This metric varies between 0 (no overlap) and 100% (identical receptive fields).

To compare the types and magnitudes of changes in receptive fields evoked by cooling different cortical areas (7b vs. 5L vs. M1/PM), several global measures of response changes were considered. For the following analyses, the responses during the later cooling epochs (cool, rewarm 1, rewarm 2) were each compared to responses during the baseline epoch. First, the proportion of recording sites exhibiting a certain type of receptive field change [expansion, contraction, or no (<5%) change] was compared with the Freeman-Halton extension of Fisher’s exact test, since the low expected frequency of certain changes precluded the use of a  $\chi^2$ -analysis. For each later temperature epoch, three separate  $2 \times 3$  (type of change  $\times$  cooled area) contingency tables were constructed to compare the proportion of sites showing a given type of change (e.g., expansion) relative to all other possible changes (i.e., contraction or no change) after the cooling of each area (5L, 7b, and M1/PM). Effect sizes were calculated if a significant relationship ( $P < 0.05$ ) between the cooled region and type of change was found.

The mean change of receptive field area following the cooling of each area was compared with a two-sample bootstrap test for unequal variances (Good 2005). This was done in lieu of a two-sample *t*-test since the assumption of normality could not be met for this measure. For comparisons between epochs, bootstrap samples of the change in receptive field size were drawn at random from the pool of sites examined with each cooled region until each cooled region’s sample was equal to the number of sites tested during cooling of that region. The difference in mean change in receptive field size between the two

cooled regions was then calculated. This procedure was repeated 5,000 times to construct a distribution of differences in receptive field size changes between the two cooled regions. If a difference of 0 was found within a 97.5% confidence interval of this distribution (2-tailed test), the null hypothesis (that the means of the 2 cooled regions did not differ) was accepted. Otherwise, it was rejected, and the mean changes in receptive field size of the two cooled regions were deemed significantly different. The mean change in receptive field size for each cooled region was compared pairwise in this manner with a Bonferroni correction for multiple comparisons (i.e., 3 comparisons at a 99.17% confidence interval). An identical procedure was used to compare differences in overlap index for each cooled region.

#### RESULTS

We tested multiunit neural responses at 112 sites in area 1, 93 sites in area 2, and 65 on the border between the two areas in six anesthetized monkeys. To determine the somatosensory receptive field, the skin and hair were stimulated manually, with a paintbrush and/or with a thin wooden probe. Of all 270 sites tested, 55 (30 in area 1, 9 in area 2, 16 on the border) were examined in detail. These 55 sites examined with cooling were limited to those with a strong neural response to cutaneous stimulation on the distal forelimb such that the receptive field could be determined unambiguously. Fisher’s exact test (recording site  $\times$  type of response change) revealed no significant relationship between the area recorded from and the type of response changes observed during cooling ( $P = 0.69$ ), so for most analyses the data were combined and are referred to as area 1/2. The distribution of sites across areas 1 and 2 and whether they were affected by cooling is illustrated in Fig. 3C, Fig. 4, *B* and *C*, and Fig. 5. Responses of neurons at each site were tested before, during, and after cooling of one or more neighboring fields (areas 5L and 7b and M1/PM). Receptive field extent was assessed via stimulation with isoforce von Frey fibers.

Among the 55 sites studied, 20 were tested for area 5L cooling, 40 for 7b cooling, and 12 for M1/PM cooling. Some sites were tested during cooling of multiple, successive areas; hence the sum of such “deactivation tests” (72; see Table 1) is more than the 55 sites tested (Table 2). Table 1 shows the numbers of deactivation tests studied during cooling, broken down by case, field cooled, and the proportion of sites at which we observed changes in receptive fields during cooling. Baseline receptive field location and configuration were determined in the first epoch, and receptive fields for subsequent epochs were compared with this baseline receptive field (see Fig. 3B). Cooling and rewarming of different regions impacted receptive field size and configuration in different ways. We analyzed this effect using two metrics: 1) receptive field size and 2) receptive field overlap.

#### *Changes in Size of Receptive Fields*

Changes in receptive field size were determined by comparing cooling and rewarming epochs with the baseline epoch. Representative examples are shown in Fig. 7. While in some instances no change in receptive field size was noted for neurons at the recording site when other cortical areas were cooled and rewarmed (Fig. 7, *top*), in about half of the sites studied we did observe alterations in the size of the receptive field as a result of cooling. An example of one of the larger changes we observed is shown in Fig. 7, *middle*. Initially, the

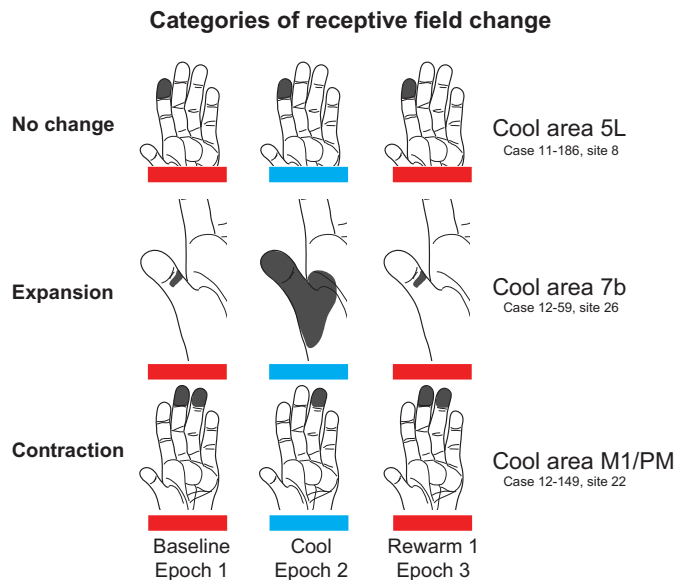


Fig. 7. Exemplars of the categories of RF change induced by cooling different areas on the RF for neurons in area 1/2. The first category is no change (top; case 11-186); the second category is an expansion (middle; case 12-59); and the third category is a contraction (bottom; case 12-149). Although not always the case, in these examples the RFs returned to baseline condition after rewarming of cooled tissue.

neurons had a small receptive field on proximal D1. During the cooling of 7b (epoch 2) the receptive field expanded 27-fold to include all of glabrous D1, portions of pad 1, and portions of the thenar pad. When cortex was rewarmed (epoch 3), the receptive field returned to its baseline configuration. A contraction of a receptive field is illustrated in Fig. 7, bottom. In this instance, the baseline receptive field was on distal D3 and D4. During cooling of M1, the receptive field was on distal D4 only, decreasing in area by 60%. After rewarming, the receptive field returned to its baseline configuration.

The dynamics of these receptive field changes were examined over the course of several long, stable recording sessions in which areas 7b and 5L and M1/PM were cooled sequentially. Within each session, the receptive field for neurons at a single site was examined (Fig. 8, A and B). In the example given in Fig. 8A, the initial receptive field was on hairy D2. During cooling and rewarming of area 7b, there was no change in the response. Subsequently at the same site, during cooling of area 5L, the receptive field expanded to D3. During rewarming, the response returned to the original extent. Finally, no change was observed during cooling and rewarming of M1/PM. Thus cooling different areas had different effects on this particular area 1/2 receptive field: 7b, no change; 5L, expansion; M1/PM, no change. The same set of cooling treatments, however, caused a different combination of effects at other recording sites. For example, at a more medial site in the same animal, the baseline receptive field was on hairy D5 (Fig. 8B). During cooling of area 7b it expanded onto hairy D4 and remained expanded during the rewarming. There was no change when area 5L was cooled, but the receptive field did expand further when area M1/PM was cooled. After rewarming, the receptive field contracted to its original size and location on hairy D5. Thus, in this same animal at a different site more distant from 7b and M1/PM, cooling 7b caused expansion, subsequent cooling of area 5L caused no change,

and subsequent cooling of M1/PM caused a large expansion in the receptive field. At both sites, rewarming largely restored the baseline receptive field (Fig. 8, A and B). An alternative interpretation would be that, rather than causing no further change, cooling 5L maintained the expanded receptive field observed after rewarming 7b and that, in the absence of 5L cooling, the receptive field would have eventually contracted back to the original location on hairy D5.

To maximize the number of sites studied, we generally did not repeat cooling of the same region while studying the same site. One exception is shown in Fig. 8C and serves as a control. During the first cycle of cooling 7b, the baseline receptive field on distal D2–3 expanded onto the entirety of glabrous D2–3. During rewarming, the receptive field contracted onto all of D3 and remained unchanged in epoch 4 (rewarm 2). Eighteen minutes after that, the receptive field had returned to a configuration similar to that of the initial baseline. During the second cooling of 7b, the receptive field expanded to all of glabrous D2–3, identical to the first cooling cycle for this site. Upon rewarming, the receptive field contracted to distal and middle D2–3, testing 5 min later revealed no further changes in the receptive field. While some differences in the two cooling cycles are evident, the general pattern and even some of the details of the expansion and contraction are similar.

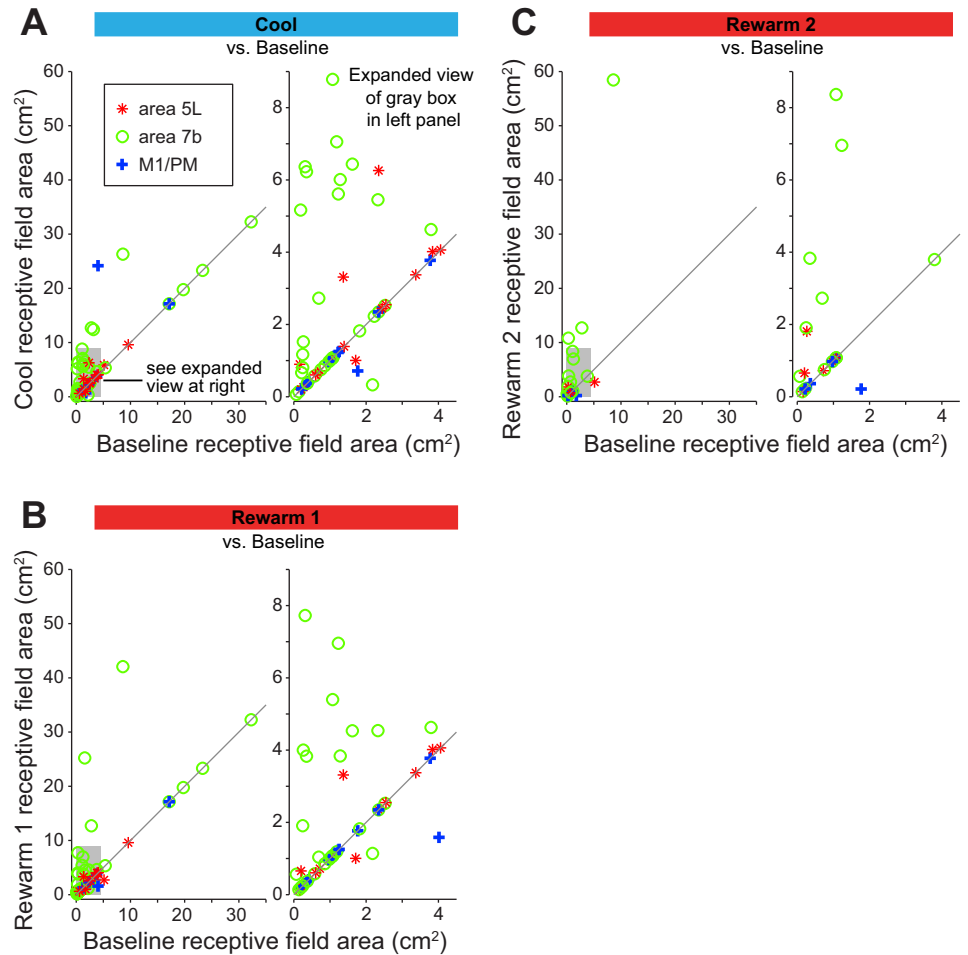
At some sites we conducted sham cooling in which the receptive field was retested after an interval comparable to that in cooling experiments, but without cooling (Fig. 8, D and E). Sham cooling did not result in changes in receptive fields, suggesting that in the absence of cooling receptive fields remain stable.

For each site tested with cooling, Fig. 9 compares the baseline area of the receptive field ( $x$ -axis) with the receptive field area during the cooling, rewarm 1, and rewarm 2 epochs ( $y$ -axis). Many sites fall along the line of equality, having shown no change in receptive field area during cooling (defined as showing  $<5\%$  change; see *Analysis of Changes in Receptive Fields*). For example, 50% of sites tested during 7b cooling showed no change in this epoch (Fig. 10A, left). There were, however, more sites with expanding than contracting receptive fields during 5L cooling (5 vs. 1; Fig. 9A) and especially during 7b cooling (18 vs. 1; Fig. 9A). Sites with expanding and contracting receptive fields fall above and below the line of equality in Fig. 9, respectively.

These findings were confirmed by the analyses shown in Fig. 10. To examine how these categories of changes were related to the area cooled, we analyzed all sites across all monkeys to determine what category of change was most prevalent. Here we report the proportion of recording sites for which cooling caused any expansion, any contraction, or no change in receptive field size. Sites with expanding receptive fields are represented as green bars in Fig. 10A; those with contraction are represented as orange bars. Of the categories of change examined, incidences of receptive field expansion were more common than contraction (Fig. 10A). Expansions were observed most frequently during cooling of 7b (47.5% of sites in the cooling epoch), less frequently during cooling of 5L (25%), and least frequently during cooling of M1/PM (8.3%). During the cool epoch we observed a significant relationship ( $P < 0.05$ , Fisher's exact test) between the area cooled and the proportion of sites in which neurons had an expansion of their receptive field, relative to the baseline epoch (Fig. 10A, left).



Fig. 9. Baseline (*x*-axis) vs. later-epoch RF area (*y*-axis) for individual recording sites. Baseline areas are compared to those of cool (A), rewarm 1 (B), and rewarm 2 (C) epochs. Panels at *right* are expanded views of the gray box in panels at *left*. Symbols indicate which area was cooled: red asterisk, area 5L; green circle, 7b; blue cross, M1/PM. Symbols above and below the line of equality indicate RF expansion and contraction, respectively.



### Receptive Field Overlap

An alternative measure of changes in receptive fields resulting from deactivation of PPC/motor fields is the overlap index (see MATERIALS AND METHODS; Merzenich et al. 1983; Padberg et al. 2010). Further examples of receptive field changes, labeled with percent overlap, are shown in Fig. 11, A–C; 100% overlap indicates a lack of change in receptive field (Fig. 11D).

As a result of 7b cooling, 51% of sites had some change in receptive field overlap. In contrast, only 30% and 17% of sites had changes in overlap during cooling of 5L and M1/PM, respectively. For comparisons of all later epochs to baseline, among sites that did show a change in overlap the magnitude of overlap was fairly evenly distributed across small and large values for 5L cooling (Fig. 11E, *left*). In contrast, when there was a change in overlap as a result of cooling and/or rewarming of 7b and M1/PM, the change was generally a large one, with overlap of <50% (Fig. 11E, *center and right*). Since receptive fields tended to expand or contract with minimal lateral shifts (i.e., one receptive field usually encompassed the other entirely, e.g., Fig. 11, A and B), measures of expansion and overlap of receptive fields are largely reciprocal, showing the same general pattern of results.

Whereas Fig. 11E displays numbers of sites with differing overlap indexes, Fig. 11F compares mean overlap index for different epochs and areas cooled. When all sites in all cases were examined, we found that the mean overlap index was lowest (indicating the greatest change in receptive field over-

lap) for 7b cooling cycles and higher for M1/PM and 5L cooling cycles (Fig. 11F, *left*). Pairwise comparisons between the different areas during the cool epoch (compared to baseline) revealed a significantly lower mean overlap index for 7b compared with 5L cooling ( $P < 0.05$ , 2-tailed test with Bonferroni correction). Pairwise comparisons between the different areas during the first rewarm epoch revealed a significantly lower mean overlap index for 7b compared with M1/PM cooling ( $P < 0.05$ ). Thus, as with comparisons of receptive field size, cooling area 7b had the largest effect on receptive fields as measured by overlap index. At a small number of sites we were able to make a direct comparison of the mean overlap index resulting from cooling all three areas, 5L, 7b, and M1/PM. There were no significant pairwise differences in overlap index between areas cooled for these seven sites (Fig. 11F, *right*), although there was a trend toward smaller receptive field overlap resulting from 7b cooling.

### DISCUSSION

Multiple studies in recent decades have shown changes in both receptive field characteristics and cortical map organization following skilled learning of a manual task in adult animals (see Kaas 1991 for review; Kleim et al. 1998; Nudo et al. 1996; Recanzone et al. 1992; Tennant et al. 2012). A prime example of the dynamic nature of cortical networks involved in hand use comes from studies in awake macaque monkeys trained to use handheld tools to retrieve food (Iriki et al. 1996).

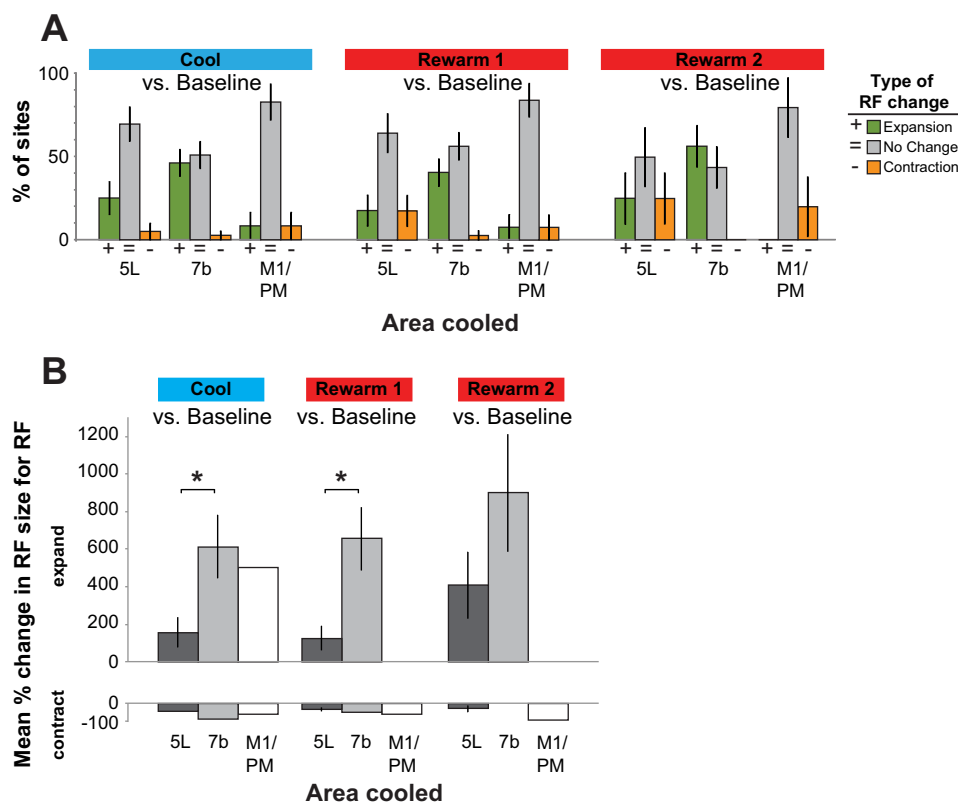


Fig. 10. *A*: proportion of sites where cooling caused expansions vs. contractions of RF size. At the majority of sites in which we cooled 5L and M1/PM we did not detect a change in RF size (gray bars). During cooling of 7b about half of the sites exhibited changes in RFs. When RFs changed, in most conditions the change was an expansion (green bars) rather than a contraction (orange bars). In the 2 rewarming epochs, the majority of sites showed no change in RF compared with baseline. However, those sites that did change generally expanded, and this was most dramatic after cooling of area 7b. This expansion of RFs persisted throughout the second rewarming epoch. *B*: mean % expansion (*top*) and contraction (*bottom*) in RF size. Means include only sites where expansion (*top*) or contraction (*bottom*) was observed. Cooling of 7b caused a significantly larger RF expansion compared with 5L during the cold and rewarm 1 epochs ( $P < 0.05$ , 2-tailed test with Bonferroni correction). Only 1 incidence of expansion was observed during M1 cooling, precluding statistical comparisons. Similarly, the low number of contractions observed as a result of cooling of each area precluded any between-area comparisons of RF contraction. All error bars are SE.

After 5 min of tool use, visual receptive fields of neurons in the anterior bank of the IPS (e.g., area 5L or MIP) that had previously encompassed the portion of visual space in which the forelimb moved expanded to encompass the portion of visual space of the forelimb plus the tool; this effect was reversible after food retrieval without the tool. A related study demonstrated that arm position-coding neurons in a similar region are susceptible to a simian version of the “rubber hand illusion” in which synchronous felt and seen stimuli on the real hand and a fake hand caused neurons to treat the fake hand as part of the body (Graziano et al. 2000). Thus fundamental features of neural receptive fields such as location on the skin or position in visual space can undergo rapid context-dependent changes. Such changes would be highly adaptive in a dynamic environment that repeatedly forced animals to solve novel sensorimotor challenges such as foraging, hunting, and social interactions.

#### Area 7b Influences on Area 1 and Area 2 Neurons

One issue that has not been actively investigated is how posterior parietal fields influence responses of neurons in hierarchically earlier cortical areas. Previous anatomical studies have shown interconnections between area 1/2 and areas 5L and 7b and thalamic nuclei (Fig. 1; Burton and Fabri 1995; Cavada and Goldman-Rakic 1989; Cooke et al. 2013; Padberg et al. 2009; Pons and Kaas 1986; Rozzi et al. 2006; Weber and Yin 1984; Yeterian and Pandya 1985), yet the function of the feedback projections have been little studied. In the present investigation we found that reversible deactivation of posterior parietal area 7b resulted in increases in receptive field size of neurons in area 1/2 in almost half of the recording sites tested, and only once resulted in a contraction. A similar result was seen for cooling area 5L:

Receptive field expansion was much more common than contraction, although 5L cooling changed a smaller proportion of receptive fields. Cooling M1/PM had a much lower incidence of influencing area 1/2 neurons (only 2 of 12 sites). These results are consistent with feedback from area 7b being primarily inhibitory, with the targets of this feedback providing inputs from the surrounding regions of skin to the area 1/2 neurons. The results demonstrate that receptive fields of neurons within this somatosensory/parietal network are highly dynamic and areas considered to be higher order can rapidly modulate neural activity in areas that provide their input directly or indirectly. Thus cortical networks involved in important and pervasive manual behaviors are apparently not organized in a strict unidirectional hierarchy from detection to perception to decision making to behavior but rather are multidirectional, interactive, and capable of rapid regulation of their inputs.

When considered separately for the three areas cooled, there was a nonsignificant trend (Fisher’s exact test,  $P = 0.15$ ) in the relationship between the recording region (area 1, area 2, and the sites on the area 1/2 border) and the incidence of cooling-related changes in receptive fields for area 7b cooling and, to a lesser extent, cooling of area 5L and M1/PM. Curiously, the proportion of sites with changes resulting from 7b cooling was greater for area 1 (13 of 20, or 65%) than for area 2 (2 of 8, or 25%), with sites on the border changing at an intermediate rate (6 of 12, or 50%). This is reversed from what one might expect given the known projections from 7b to area 2, but not to area 1 (although Burton and Fabri 1995 report there are projections to the face representation of area 1). This suggests that if disruption of feedback projections from 7b is responsible for such changes in area 1, then the connections are indirect, for example, via area 5 (Cavada and Goldman-Rakic 1989; Cooke et al. 2013; Pons and

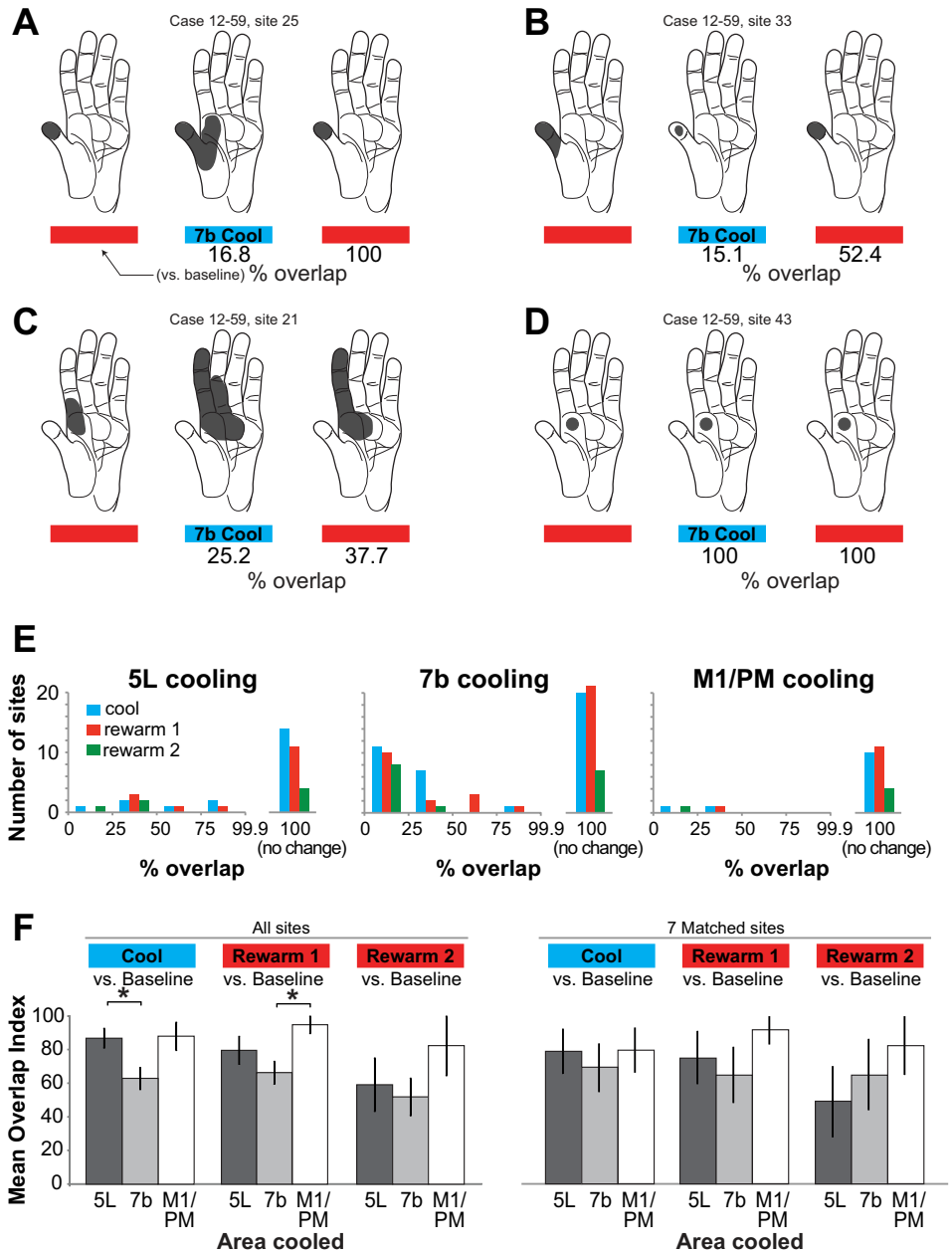


Fig. 11. Extent to which RFs overlap during cooling and rewarming of different areas. *A–D*: examples of changes in RFs and the overlap index assigned to each field. *E*: frequency of different levels of RF overlap binned into increments of 25%. Blue, cool vs. baseline; red, rewarm 1 vs. baseline; green, rewarm 2 vs. baseline. Among sites where there was a RF change, a large majority during 7b and M1/PM cooling exhibited a % overlap <50% whereas that for 5L cooling was more evenly distributed. That is, when there was a change in the RF as a result of cooling 7b and M1/PM, the change was usually substantial. In contrast, changes in area 1/2 RFs as result of 5L cooling included a mix of sites with large and smaller overlaps. *F*: in comparing baseline to later epochs (“All sites,” *left*), the mean overlap in RFs was significantly smaller (\*; i.e., there was a greater change) during 7b cooling than 5L cooling; in the initial rewarming epoch, mean overlap was significantly smaller (\*) after 7b cooling than M1/PM cooling. There was no significant difference in overlap in the second rewarming epoch as a result of cooling 5L, 7b, or M1/PM. At a small number of sites we were able to test the effect of cooling 5L, 7b, and M1/PM in succession. These 7 sites are compared on *right* (“7 Matched sites”). Error bars are SE.

Kaas 1986), area 2 (Burton and Fabri 1995; Pons and Kaas 1986; Rozzi et al. 2006), or the thalamus (Padberg et al. 2009; Weber and Yin 1984; Yeterian and Pandya 1985).

As mentioned in MATERIALS AND METHODS, 7b overlaps areas PF and PFG (see Table 3). As we were not able to identify these fields based on sulcal patterns and architectonic boundaries using Nissl stains are not particularly distinct, we do not know whether some cooling devices deactivated one more than the other. It is possible that the variability in the efficacy of 7b cooling (Table 1) stems in part from differential cooling of PF and PFG, and PF does have sparse connections with area 1 (Rozzi et al. 2006).

#### Effects of Anesthesia

All data were acquired while the animals were anesthetized. Not all receptive fields changed as a result of cooling (43.1%

changed overall); this proportion varied between animals (Table 1), but such variation was not associated with the anesthetic regime used (see *Anesthetics and Surgical Procedures*). Furthermore, when neurons at the same recording site were examined after sequentially cooling different cortical fields, receptive fields underwent changes for cooling of some areas but not others (Fig. 8). Therefore, we did not observe any evidence that anesthesia influenced the changes in receptive fields that we report here.

#### Relationship to Other Studies

To our knowledge, this is the first study that examines the effect of reversibly deactivating areas in PPC on what are considered to be very early stages of somatosensory processing at the level of areas 1 and 2. In a previous study in our laboratory, we examined the effects of lesioning posterior

Table 3. *Abbreviations*

Body parts	
D1–5	Digits 1–5
Cortical fields and structures	
1	Area 1; cutaneous representation caudal to area 3b
2	Area 2; representation of deep receptors caudal to area 1
3b	Area 3b, primary somatosensory area, S1 proper
5L	Area 5, lateral division (as defined in Seelke et al. 2012)
7b	Area 7b; posterior parietal area on inferior parietal lobule
CS	Central sulcus
IPS	Intraparietal sulcus
LS	Lateral sulcus
M1	Primary motor cortex
MIP	Medial intraparietal area
PF	Parietal area F; overlaps 7b
PFG	Parietal area FG; overlaps 7b
PM	Premotor cortex
V1	Primary visual cortex
V2	Visual area 2
V3	Visual area 3
Other abbreviations	
3D	3-Dimensional
PDMS	Polydimethylsiloxane
PBS	Phosphate-buffered saline
RF	Receptive field
mtc	Microthermocouple

parietal area 5 on the receptive fields for neurons in areas 1 and 2 (Padberg et al. 2010). While the main goal of the study was to investigate long-term consequences of such a lesion, many cortical sites were investigated within 60 min of the insult. As expected, neural responses in these adjacent fields were spared, but changes were noted in the size and location of some receptive fields. The present study extends those findings to show that a similar result can be repeatedly demonstrated in the same animal, that the changes occur over a very short time course (often within 5 min), and that such changes are more common when area 7b is inactivated compared with area 5L or M1/PM.

The present results are consistent with previous studies investigating earlier processing areas of somatosensory cortex. Reversibly deactivating portions of 3b and 1 (via cooling) on callosally connected neurons in 3b of megachiropteran bats (Clarey et al. 1996) also results in an expansion of receptive fields, in this case for neurons in area 3b in the opposite hemisphere. Also of interest are several studies demonstrating that manipulation or deactivation of motor cortex in monkeys (Sasaki and Gemba 1984) and rodents (Lee et al. 2008, 2013; Pais-Vieira et al. 2013; Zagha et al. 2013) modulated activity in somatosensory cortex [for further discussion of motor cortical feedback, see companion article (Goldring et al. 2014)]. While we observed smaller effects on area 1/2 receptive fields when cooling M1/PM compared with areas 7b or 5L, these data are consistent with these studies of motor-somatosensory feedback.

What mechanism might be responsible for the expansion of receptive fields we and others have observed? One interpretation is that area 7b normally inhibits inputs to area 1/2 neurons that are responsive to the receptive field surround (and possibly the center as well). Cooling disrupts this feedback inhibition,

leading to observed receptive field expansion. Given the receptive field mapping techniques used here, it is not possible to say whether the receptive field surrounds were inhibitory—suppressing responses in the center, merely silent, or part of a more complex feature-detector typical of neurons in anterior parietal cortex (Gardner and Costanzo 1980a, 1980b, 1980c; Hyvärinen and Poranen 1978; Sur 1980). While the mechanism responsible for the receptive field alteration is unknown, the general finding that PPC fields influence anterior parietal somatosensory area neurons outside of their receptive field center is consistent with similar studies in the visual system of monkeys (Nassi et al. 2013). Reversibly deactivating V2 and V3 by cooling had little or no effect on receptive field centers of V1 neurons but caused a substantial decrease in surround suppression and reduced orientation selectivity. These findings suggest that inhibitory feedback from V2 and V3 contributes to the spatial specificity of V1 responses. Similarly, deactivation of motion-processing fields in cats and monkeys eliminates global motion signals in V1 and/or V2 (Jansen-Amorim et al. 2011; Schmidt et al. 2011). These and other studies (Huang et al. 2007; Jansen-Amorim et al. 2012; Wang et al. 2007) suggest that spatially restricted receptive fields of neurons in V1 can incorporate information from more distant parts of the visual field in the form of surround suppression, end-stopping, or global motion. Thus, similar to the somatosensory system, information outside of the classical receptive field of a V1 neuron normally passes from higher- to lower-level fields in the form of inhibitory feedback.

The study described in our companion paper (Goldring et al. 2014) was conducted concurrently with the present study and, like it, explored responses to tactile stimuli on the hand during cooling of the same three fields (5L and 7b and M1/PM). The two studies used distinct stimuli and methodology to provide complementary data sets: This study emphasized spatial detail (hand mapping), while the companion study emphasized temporal detail (computer-controlled stimuli). For a complete comparison of methodology and results, see the companion article (Goldring et al. 2014).

#### *Reversibility of Cooling Deactivation*

As discussed below, some changes occurring during cooling deactivation persisted after rewarming. One possible reason for this is that cooling may have generated tissue damage below the chip and thus resulted in a permanent rather than a reversible lesion. We consider this unlikely for several reasons. First, in a previous study in which the efficacy of these cooling devices was examined, we observed rapid recovery of neural activity directly under the cooling device within minutes of rewarming after multiple cooling-rewarming cycles (Figs. 10 and 11 in Cooke et al. 2012). Second, in the present study, we continued to see new effects of cooling on receptive fields in areas 1 and 2 after many cooling-rewarming cycles. If deactivation of 5L, 7b, and/or M1 was causing permanent damage, one would not expect to see effects of subsequent cooling, and would likely observe at least declining effectiveness on repeated use of each cooling chip. This was not the case; we observed changes as a result of cooling as many as eight times for a single cooling chip (Table 1). Changes were often observed on consecutive tests (of 2 different recording sites with the same cooling chip) separated by <1 h and were also

seen as much as 23 h after the first cooling test for a given cooling chip. Repeated cooling of the same region of cortex therefore did not result in decreased deactivation efficacy after short or long intervals, suggesting that cooling deactivation in this study was, in fact, reversible.

### *Persistence of Receptive Field Changes*

An important observation from the present investigation is that the receptive fields of neurons at some sites returned to baseline during the rewarm epochs, while at other sites changes that appeared during cooling persisted or even increased. Indeed, both the proportion of sites where there was some change (Fig. 10A) and the mean change in receptive field size (Fig. 10B) were greater after rewarming than during cooling. Moreover, our second test after rewarming (rewarm 2) often revealed that receptive fields continued to change after cortical temperature had stabilized, sometimes in a direction further from the baseline size. Similar effects of rewarming have been documented by other groups (see Goldring et al. 2014 for a brief review).

First, we must consider whether these changes are likely to be permanent. At most sites we did not test beyond the rewarm 2 epoch, 19–24 min after cooling ceased. However, on the occasions when we did define the receptive field after longer intervals (Fig. 8C) and in cases where we cooled and rewarmed other cortical fields (Fig. 8B) we often saw that receptive fields returned to baseline or much closer to it than during earlier rewarm epochs. In light of these examples, it is possible that if we continued testing for prolonged durations, all receptive fields would have eventually returned to their baseline state. This would indicate that neurons in the regions we explored can react to cooling and rewarming with different time courses.

Cooling and rewarming may have initiated changes in existing circuitry or set in motion a cascade of changes in functional connectivity that decay on a longer timescale, or not at all. Experiments in slice preparations have demonstrated that rewarming of neural tissue in a temperature range similar to that used in this study produced increases in tissue excitability (Aihara et al. 2001; Volgushev et al. 2004), although by itself this would seem likely to reverse rather than continue and sometimes enhance effects of cooling. Rather, by substantially altering the activity of these cortical networks during cooling, we altered (perhaps irreversibly) the efficacy of existing synapses, thereby changing both neural response properties as well as receptive field characteristics in the areas in which our recordings were made. We only examined receptive fields in areas 1 and 2, but it is likely that additional changes in neural response properties would be observed in the cooled areas and across the network of somatosensory fields (Fig. 1).

### *Functional Implications*

**Persistent changes.** Our relatively large manipulation of these cortical circuits may reveal what is naturally occurring on a local scale, minute by minute, across the entire cortical sheet in awake, behaving animals. Rapid alterations to circuits occur continuously as the cortex confronts novel patterns of sensory stimulation in a complex environment. In this scenario, there is nothing permanent about the “baseline” state of area 1/2 receptive fields we observed before each cooling test. Instead, rather than returning to a previous state after a perturbation,

these dynamic circuits are continuously updated based on current sensory context (which generates unique patterns of cortical activity) and at any two moments in time are never the same.

**Top-down influence.** We find that the perturbation of neurons in what is traditionally considered a high-order cortical field (area 7b) has profound effects on the responses of neurons in early cortical areas (area 1/2). This type of descending influence could serve multiple functional roles, including shaping early neural responses as a function of the ethological context, previous history, attention and/or arousal, or task demands. Hand use in primates presents complex and relatively unique demands on the somatosensory and motor systems compared with other body parts and may need to be controlled by a rapidly dynamic and flexible cortical circuit. If so, such circuitry would be expected in similar systems in other species, such as hand use in humans, as well as the control of the lips, jaw, tongue, and supralaryngeal structures necessary for human speech. Alternatively, this type of dynamic and flexible circuit may be the basic processing strategy of the cerebral cortex, with differences between systems and species based on the number of cortical fields and degree of interconnectedness. Taken in this context, these two possibilities are not mutually exclusive but may be better revealed in certain systems compared with others.

### ACKNOWLEDGMENTS

We thank Conor Weatherford, Adam Gordon, Syed Hussain, Becky Grunewald, and Hoang Nguyen for assistance with data collection and analysis.

### GRANTS

This work was supported by National Institutes of Health Grants R01 NS-035103 and R21 EB-012866 to L. Krubitzer and Vision Training Grant T32EY-015387 to A. B. Goldring and M. K. L. Baldwin.

### DISCLOSURES

No conflicts of interest, financial or otherwise, are declared by the author(s).

### AUTHOR CONTRIBUTIONS

Author contributions: D.F.C., A.B.G., G.H.R., and L.K. conception and design of research; D.F.C., A.B.G., M.K.L.B., G.H.R., and L.K. performed experiments; D.F.C., A.B.G., and M.K.L.B. analyzed data; D.F.C., A.B.G., G.H.R., and L.K. interpreted results of experiments; D.F.C., A.B.G., M.K.L.B., and L.K. prepared figures; D.F.C., A.B.G., and L.K. drafted manuscript; D.F.C., A.B.G., M.K.L.B., G.H.R., A.C., T.P., S.I.S., and L.K. edited and revised manuscript; D.F.C., A.B.G., and L.K. approved final version of manuscript.

### REFERENCES

- Aihara H, Okada Y, Tamaki N.** The effects of cooling and rewarming on the neuronal activity of pyramidal neurons in guinea pig hippocampal slices. *Brain Res* 893: 36–45, 2001.
- Burton H, Fabri M.** Ipsilateral intracortical connections of physiologically defined cutaneous representations in areas 3b and 1 of macaque monkeys: projections in the vicinity of the central sulcus. *J Comp Neurol* 355: 508–538, 1995.
- Cavada C, Goldman-Rakic PS.** Posterior parietal cortex in rhesus monkey. I. Parcellation of areas based on distinctive limbic and sensory corticocortical connections. *J Comp Neurol* 287: 393–421, 1989.
- Clarey JC, Tweedale R, Calford MB.** Interhemispheric modulation of somatosensory receptive fields: evidence for plasticity in primary somatosensory cortex. *Cereb Cortex* 6: 196–206, 1996.

- Cooke DF, Goldring AB, Yamayoshi I, Tsourkas P, Recanzone GH, Tiriach A, Pan T, Simon SI, Krubitzer L. Fabrication of an inexpensive, implantable cooling device for reversible brain deactivation in animals ranging from rodents to primates. *J Neurophysiol* 107: 3543–3558, 2012.
- Cooke DF, Padberg J, Cerkevich CM, Kaas JH, Krubitzer L. Corticocortical connections of area 5 in macaque monkeys support the existence of functionally distinct medial and lateral regions (Abstract). *2013 Neuroscience Meeting Planner*. Program No. 551.09, 2013.
- Ergenzinger ER, Glasier MM, Hahm JO, Pons TP. Cortically induced thalamic plasticity in the primate somatosensory system. *Nat Neurosci* 1: 226–229, 1998.
- Gardner EP, Costanzo RM. Neuronal mechanisms underlying direction sensitivity of somatosensory cortical neurons in awake monkeys. *J Neurophysiol* 43: 1342–1354, 1980a.
- Gardner EP, Costanzo RM. Spatial integration of multiple-point stimuli in primary somatosensory cortical receptive fields of alert monkeys. *J Neurophysiol* 43: 420–443, 1980b.
- Gardner EP, Costanzo RM. Temporal integration of multiple-point stimuli in primary somatosensory cortical receptive fields of alert monkeys. *J Neurophysiol* 43: 444–468, 1980c.
- Ghazanfar AA, Krupa DJ, Nicolelis MA. Role of cortical feedback in the receptive field structure and nonlinear response properties of somatosensory thalamic neurons. *Exp Brain Res* 141: 88–100, 2001.
- Ghosh S, Murray GM, Turman AB, Rowe MJ. Corticothalamic influences on transmission of tactile information in the ventroposterolateral thalamus of the cat: effect of reversible inactivation of somatosensory cortical areas I and II. *Exp Brain Res* 100: 276–286, 1994.
- Goldring AB, Cooke DF, Baldwin MK, Recanzone GH, Gordon AG, Pan T, Simon SI, Krubitzer L. Reversible deactivation of higher-order posterior parietal areas. II. Alterations in response properties of neurons in areas 1 and 2. *J Neurophysiol* (August 20, 2014) doi:10.1152/jn.00141.2014.
- Good PI. *Resampling Methods: A Practical Guide to Data Analysis*. Boston, MA: Birkhäuser, 2005.
- Graziano MS, Cooke DF, Taylor CS. Coding the location of the arm by sight. *Science* 290: 1782–1786, 2000.
- Gregoriou GG, Borra E, Matelli M, Luppino G. Architectonic organization of the inferior parietal convexity of the macaque monkey. *J Comp Neurol* 496: 422–451, 2006.
- Huang JY, Wang C, Dreher B. The effects of reversible inactivation of postero-temporal visual cortex on neuronal activities in cat's area 17. *Brain Res* 1138: 111–128, 2007.
- Hyvärinen J, Poranen A. Function of the parietal associative area 7 as revealed from cellular discharges in alert monkeys. *Brain* 97: 673–692, 1974.
- Hyvärinen J, Poranen A. Receptive field integration and submodality convergence in the hand area of the post-central gyrus of the alert monkey. *J Physiol* 283: 539–556, 1978.
- Iriki A, Tanaka M, Iwamura Y. Coding of modified body schema during tool use by macaque postcentral neurons. *Neuroreport* 7: 2325–2330, 1996.
- Iwamura Y. Hierarchical somatosensory processing. *Curr Opin Neurobiol* 8: 522–528, 1998.
- Jansen-Amorim AK, Fiorani M, Gattass R. GABA inactivation of area V4 changes receptive-field properties of V2 neurons in Cebus monkeys. *Exp Neurol* 235: 553–562, 2012.
- Jansen-Amorim AK, Lima B, Fiorani M, Gattass R. GABA inactivation of visual area MT modifies the responsiveness and direction selectivity of V2 neurons in Cebus monkeys. *Vis Neurosci* 28: 513–527, 2011.
- Kaas JH. Plasticity of sensory and motor maps in adult mammals. *Annu Rev Neurosci* 14: 137–167, 1991.
- Kambi N, Tandon S, Mohammed H, Lazar L, Jain N. Reorganization of the primary motor cortex of adult macaque monkeys after sensory loss resulting from partial spinal cord injuries. *J Neurosci* 31: 3696–3707, 2011.
- Kleim JA, Barbay S, Nudo RJ. Functional reorganization of the rat motor cortex following motor skill learning. *J Neurophysiol* 80: 3321–3325, 1998.
- Lee S, Carvell GE, Simons DJ. Motor modulation of afferent somatosensory circuits. *Nat Neurosci* 11: 1430–1438, 2008.
- Lee S, Kruglikov I, Huang ZJ, Fishell G, Rudy B. A disinhibitory circuit mediates motor integration in the somatosensory cortex. *Nat Neurosci* 16: 1662–1670, 2013.
- Leinonen L, Hyvärinen J, Nyman G, Linnankoski I. I. Functional properties of neurons in lateral part of associative area 7 in awake monkeys. *Exp Brain Res* 34: 299–320, 1979.
- Lewis J, Van Essen D. Mapping of architectonic subdivisions in the macaque monkey, with emphasis on parieto-occipital cortex. *J Comp Neurol* 428: 79–111, 2000.
- Merzenich MM, Kaas JH, Wall JT, Sur M, Nelson RJ, Felleman DJ. Progression of change following median nerve section in the cortical representation of the hand in areas 3b and 1 in adult owl and squirrel monkeys. *Neuroscience* 10: 639–665, 1983.
- Mountcastle VB, Lynch JC, Georgopoulos A, Sakata H, Acuna C. Posterior parietal association cortex of the monkey: command functions for operations within extrapersonal space. *J Neurophysiol* 38: 871–908, 1975.
- Nassi JJ, Lomber SG, Born RT. Corticocortical feedback contributes to surround suppression in V1 of the alert primate. *J Neurosci* 33: 8504–8517, 2013.
- Nelson RJ, Sur M, Felleman DJ, Kaas JH. Representations of the body surface in postcentral parietal cortex of *Macaca fascicularis*. *J Comp Neurol* 192: 611–643, 1980.
- Nudo RJ, Milliken GW, Jenkins WM, Merzenich MM. Use-dependent alterations of movement representations in primary motor cortex of adult squirrel monkeys. *J Neurosci* 16: 785–807, 1996.
- Orban GA. Higher order visual processing in macaque extrastriate cortex. *Physiol Rev* 88: 59–89, 2008.
- Padberg J, Cerkevich C, Engle J, Rajan AT, Recanzone G, Kaas J, Krubitzer L. Thalamocortical connections of parietal somatosensory cortical fields in macaque monkeys are highly divergent and convergent. *Cereb Cortex* 19: 2038–2064, 2009.
- Padberg J, Recanzone G, Engle J, Cooke D, Goldring A, Krubitzer L. Lesions in posterior parietal area 5 in monkeys result in rapid behavioral and cortical plasticity. *J Neurosci* 30: 12918–12935, 2010.
- Pais-Vieira M, Lebedev MA, Wiest MC, Nicolelis MA. Simultaneous top-down modulation of the primary somatosensory cortex and thalamic nuclei during active tactile discrimination. *J Neurosci* 33: 4076–4093, 2013.
- Pandya DN, Seltzer B. Intrinsic connections and architectonics of posterior parietal cortex in the rhesus monkey. *J Comp Neurol* 204: 196–210, 1982.
- Pons TP, Garraghty PE, Cusick CG, Kaas JH. The somatotopic organization of area 2 in macaque monkeys. *J Comp Neurol* 241: 445–466, 1985.
- Pons TP, Kaas JH. Corticocortical connections of area 2 of somatosensory cortex in macaque monkeys: a correlative anatomical and electrophysiological study. *J Comp Neurol* 248: 313–335, 1986.
- Preuss TM, Goldman-Rakic PS. Architectonics of the parietal and temporal association cortex in the strepsirrhine primate *Galago* compared to the anthropoid primate *Macaca*. *J Comp Neurol* 310: 475–506, 1991.
- Recanzone GH, Merzenich MM, Jenkins WM, Grajski KA, Dinse HR. Topographic reorganization of the hand representation in cortical area 3b of owl monkeys trained in a frequency discrimination task. *J Neurophysiol* 67: 1031–1056, 1992.
- Rozzi S, Calzavara R, Belmalih A, Borra E, Gregoriou GG, Matelli M, Luppino G. Cortical connections of the inferior parietal cortical convexity of the macaque monkey. *Cereb Cortex* 16: 1389–1417, 2006.
- Rozzi S, Ferrari PF, Bonini L, Rizzolatti G, Fogassi L. Functional organization of inferior parietal lobule convexity in the macaque monkey: electrophysiological characterization of motor, sensory and mirror responses and their correlation with cytoarchitectonic areas. *Eur J Neurosci* 28: 1569–1588, 2008.
- Sasaki K, Gamba H. Compensatory motor function of the somatosensory cortex for the motor cortex temporarily impaired by cooling in the monkey. *Exp Brain Res* 55: 60–68, 1984.
- Schmidt KE, Lomber SG, Payne BR, Galuske RA. Pattern motion representation in primary visual cortex is mediated by transcortical feedback. *Neuroimage* 54: 474–484, 2011.
- Seelke AM, Padberg JJ, Disbrow E, Purnell SM, Recanzone G, Krubitzer L. Topographic maps within Brodmann's area 5 of macaque monkeys. *Cereb Cortex* 22: 1834–1850, 2012.
- Sur M. Receptive fields of neurons in areas 3b and 1 of somatosensory cortex in monkeys. *Brain Res* 198: 465–471, 1980.
- Sur M, Wall JT, Kaas JH. Modular distribution of neurons with slowly adapting and rapidly adapting responses in area 3b of somatosensory cortex in monkeys. *J Neurophysiol* 51: 724–744, 1984.
- Tennant KA, Adkins DL, Scalco MD, Donlan NA, Asay AL, Thomas N, Kleim JA, Jones TA. Skill learning induced plasticity of motor cortical representations is time and age-dependent. *Neurobiol Learn Mem* 98: 291–302, 2012.
- Volgushev M, Kudryashov I, Chistiakova M, Mukovski M, Niesmann J, Eysel UT. Probability of transmitter release at neocortical synapses at different temperatures. *J Neurophysiol* 92: 212–220, 2004.

**Wang C, Waleszcyk WJ, Burke W, Dreher B.** Feedback signals from cat's area 21a enhance orientation selectivity of area 17 neurons. *Exp Brain Res* 182: 479–490, 2007.

**Weber JT, Yin TC.** Subcortical projections of the inferior parietal cortex (area 7) in the stump-tailed monkey. *J Comp Neurol* 224: 206–230, 1984.

**Yeterian EH, Pandya DN.** Corticothalamic connections of the posterior parietal cortex in the rhesus monkey. *J Comp Neurol* 237: 408–426, 1985.

**Zagha E, Casale AE, Sachdev RN, McGinley MJ, McCormick DA.** Motor cortex feedback influences sensory processing by modulating network state. *Neuron* 79: 567–578, 2013.

